Linear and Nonlinear Optical Characterization of a Tetraphenylporphyrin−Carbon Nanotube Composite System

Éimhín M. Ní Mhuircheartaigh, Silvia Giordani, and Werner J. Blau*

School of Physics, Trinity College Dublin, Dublin 2, Ireland

Received: June 8, 2006; In Final Form: September 6, 2006

We present a study of tetraphenylporphyrin composites formed with single-walled carbon nanotubes (SWNTs). Stable porphyrin/SWNT composite solutions were obtained by non-covalent bonding between the carbon nanotubes and conjugated tetraphenylporphyrin molecules. Transmission electron microscopy reveals porphyrin molecules adhering to the nanotube surface. We report on the first complete linear and nonlinear optical characterization of these nanocomposite materials. The composite solutions were found to be superior optical limiters to nanotubes alone, and to all porphyrin systems studied, including metalloporphyrins.

Introduction

Single-walled carbon nanotubes (SWNTs) possess unique structural, mechanical, and electronic properties, and are thus promising materials for future device fabrication. However, their potential is limited in that they are insoluble in aqueous and organic solutions, and satisfactory control over nanotube location and orientation has yet to be achieved. SWNT solubility has recently been achieved by functionalizing them covalently and noncovalently. Noncovalent functionalization is of particular interest because it provides a method of handling the nanotubes chemically without altering the electronic structure of the nanotubes themselves, and this has been achieved in a number of ways.[1−5] Porphyrins are an important family of conjugated organic molecules, whose members include many important biochemical compounds such as hemoglobin and chlorophyll, and have applications in many industries including medicine, optics, and electronics. Porphyrins are used in cancer photodynamic therapy, sensitizers for photoactive switches, artificial photosynthesis studies, and electronics. By functionalizing SWNTs with porphyrins, the nanotubes may acquire many of the intrinsic porphyrin properties such as luminescence and biocompatibility.

Studies on the optical nonlinear properties of organic molecules with extensive π electron delocalization have drawn considerable attention for a long time because of their large and fast nonlinear optical response and capability to be readily engineered for a particular purpose. Among these molecules, porphyrins are one of the most studied classes of compounds because of their importance and abundance in nature. Photonic optical limiting devices capable of controlling the amplitude gain or extinction of optical beams are required for the protection of sensors and eyes from energetic light pulses. Because of their large π-conjugated systems, the optical nonlinear properties of many organic materials, including members of the porphyrin and phthalocyanine families, have been studied in order to develop such devices for optical limiting applications.[6,7] Reverse saturable absorption (RSA) in porphyrins was first reported by Blau et al.[8] for laser pulses at 532 nm with 80 ps duration. The excited-state absorption cross-section, σ_{ex}, was found to be larger than the ground-state absorption cross-section, σ_g, for a series of tetraphenylporphyrin (TPP) derivatives. Much work has subsequently been carried out on improving the optical limiting properties of porphyrins and metalloporphyrins. It has been shown that SWNTs and multiwalled nanotubes (MWNTs) in suspension excited with high intensity at 532 and 1064 nm also behave as optical limiters.[9−11] This nonlinear behavior has been shown to arise from strong nonlinear scattering due to the creation of new scattering centers by ionized carbon microplasmas and solvent microbubbles. Improved optical nonlinear behavior is therefore to be expected from porphyrin−SWNT composite solutions, with an additional scattering component expected to enhance the nonlinear optical limiting behavior of the porphyrin macrocycle.

Thus, the optical properties of carbon nanotubes noncovalently functionalized with porphyrin molecules are of great interest in both the linear and nonlinear regimes. We report here on the photophysical and nonlinear optical properties of porphyrin molecules and their SWNT composites. In addition to this, for the first time we also clarify the discrepancies in optical absorption and fluorescence spectra reported by others.

Experimental Methods

The purified SWNTs used in this work were prepared by the HiPCO process,[13] supplied by Carbon Nanotechnologies, Inc., and used without further treatment. The TPP, zinc-TPP (ZnTPP), and protoporphyrin IX (PPIX) molecules used were purchased from Aldrich. Two identical sets of solutions of each porphyrin were made with concentrations ranging from approximately 1 to 200 μM in chloroform and dimethylformamide (DMF). Pure HiPCO SWNTs were added to one porphyrin solution at each concentration such that the porphyrin−SWNT mass ratio was 1:1.

Photoluminescence (PL) measurements were carried out using an LS-55 Perkin-Elmer luminescence spectrometer with an excitation wavelength equal to the absorption maximum of the porphyrin in question for each solvent. The linear absorption spectra were recorded using a Shimadzu UV3100 UV-visible/near-infrared (UV−vis−NIR) spectrometer.

The open aperture *z*-scan technique was used for the nonlinear optical experiments. In this experiment, the sample is scanned through the focus of a Gaussian laser beam. Initially, the beam energy density is low, and hence negligible nonlinear activity

* To whom correspondence should be addressed. E-mail: wblau@tcd.ie.

10.1021/jp063562z CCC: $33.50
Published on Web 10/24/2006

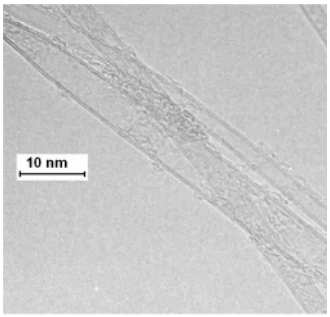

Figure 1. TEM image showing the adhesion of organic porphyrin molecules to the outside of Nanocyl double-walled nanotubes (DWNTs). DWNTs were chosen due to their improved contrast for TEM imaging. The image above was taken for a 2:1 ZnTPP/DWNT composite at a high concentration of 0.02 kg m^{-3} in chloroform.

occurs. As the sample approaches the focus, the beam diameter decreases, and thus the energy density increases, exciting the nonlinear activity within the sample medium. After the focus, the optical activity tends toward the linear regime again as the beam diameter increases with a corresponding energy density decrease. The measured beam transmittance as a function of position from the focus constitutes the open aperture *z*-scan spectra from which the nonlinear extinction coefficient can be extracted. Effective absorption coefficients and hence the imaginary third-order optical susceptibility $\mathrm{Im}\{\chi^{(3)}\}$, were calculated by following ref 18. All experiments described in this study were performed using 6 ns Gaussian pulses from a Q-switched Nd:YAG laser with energies of approximately 0.2−0.3 mJ per pulse. The beam was spatially filtered to remove the higher order modes and tightly focused. The laser was operated at its second harmonic, 532 nm, with a pulse repetition rate of 10 Hz. All linear and nonlinear optical measurements were performed in 1 cm^2 quartz cells.

Results and Discussion

The HiPCO SWNT were found to be completely insoluble in chloroform and fell out of solution at all concentrations within minutes. Limited solubility was observed for SWNT in DMF for concentrations below 0.01 g L^{-1}. In both solvents, it was found that TPP and its zinc metalloporphyrin derivative ZnTPP could disperse SWNTs. No precipitation was noticed in the TPP/SWNT and ZnTPP/SWNT solutions, even after several months of storage.

Because of their high degree of conjugation, porphyrin molecules are expected to bind noncovalently to carbon nanotubes through van der Waals interactions. These noncovalently functionalized porphyrin−carbon nanotube composites were observed by transmission electron microscopy (TEM) (Figure 1) where the amorphous ZnTPP molecules can clearly be seen adhering to the nanotube surface.

An improvement in SWNT solubility in DMF was confirmed by the intensity increase of the Van Hove peaks for the composite solutions using UV−vis−NIR absorption spectroscopy (Figure 2). Upon interaction with the carbon nanotubes, no change in the TPP absorption spectrum is observed, with the composite displaying peaks originating from both the porphyrin molecules (417, 513.5, 548, 590, and 646 nm) and carbon nanotubes (741, 812.5,1177, 1314, and 1430 nm). The carbon nanotube Van Hove absorption peaks at 377, 409, 451, 504, 559, 602, and 658 nm are too weak to be observed in the composite spectrum and are masked by the stronger TPP absorption. The Soret band absorption at 417 nm is unchanged and is too strong to be observed at the scale in Figure 2.

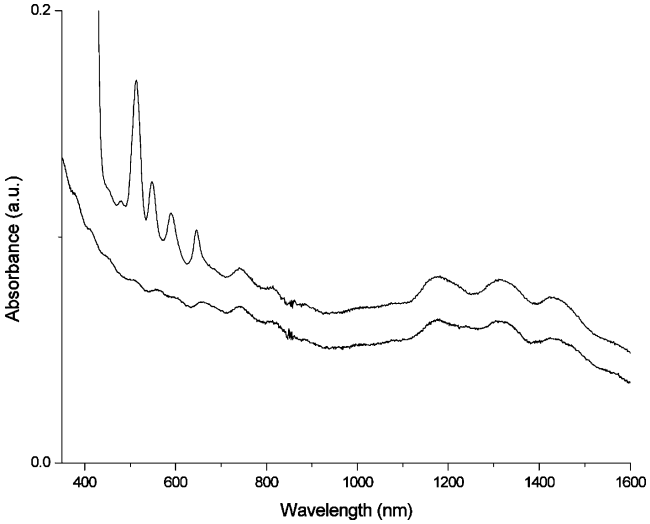

Figure 2. UV−vis−NIR absorption spectra of SWNTs in DMF (black) and TPP/SWNT composites (gray) (2.9 μM, DMF, 25 °C). The increased solubility of the SWNT in the presence of the porphyrins is confirmed by the increased absorption of the nanotube Van Hove peaks.

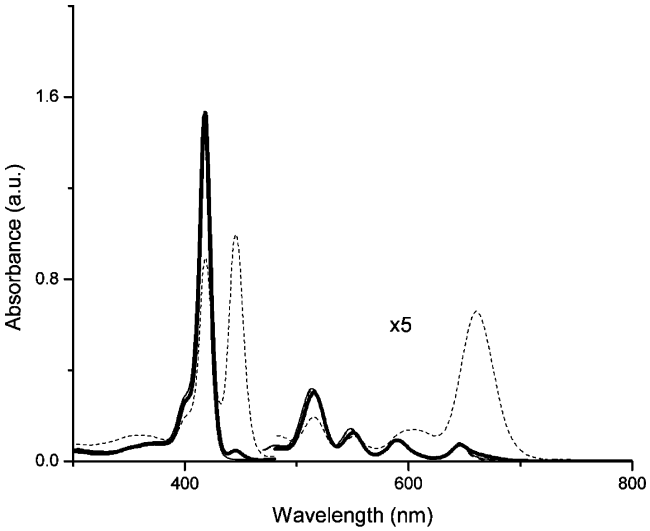

Figure 3. The absorption spectrum of TPP before (solid lines) and after (dashed lines) sonication for 30 s in chloroform (black) and DMF (gray) (3.3 μM, $CHCl_3$, 25 °C; 35.1 μM, DMF, 25 °C).

A slow aggregation of the TPP/SWNT composite solutions was noticed when the concentration of the dispersion was greater than 59 μM. The TPP and ZnTPP molecules in chloroform both displayed typical absorption spectra, with Soret bands observed at 418 and 422 nm, respectively. However, upon the introduction of energy into the system in the form of sonication or intense irradiation during *z*-scan, the Soret band split (Figure 3), with a second absorption band appearing at the longer wavelength of 446 nm. Introduction of the nanotubes into this system did not affect the positions of these peaks. However, as sonication was necessary in order to disperse the nanotubes throughout the solution, the composite solutions always yielded this second red-shifted absorption peak. It was found that the sonodegradation of chloroform during sample preparation yielded HCl, which subsequently caused protonation of the core nitrogen atoms.[12] The absorption spectrum of the deprotonated form is characterized by four Q-bands localized at 515.5, 550, 591, and 646 nm, whereas, upon protonation, the Q-bands shift to two strong maxima at 610 and 661 nm. The green solution obtained in these conditions did not show any sign of aggregation, even after several weeks.

A splitting of the TPP Soret band in chloroform has already been observed.[14] In that study, Baskaran et al. attributed the unusual absorption spectra to the interaction of residual acid groups on the surface of the carbon nanotubes with the porphyrin molecules and their subsequent covalent linkage onto the nanotube surface. However, since we have observed the same effects in the absence of nanotubes, the validity of this hypothesis must be called into question.

Once the absorption and the concentration were measured, the ground-state absorption cross-section σ_g was found from the relation $\alpha_g = N\sigma_g$, where α_g is the ground-state absorption coefficient and N is the molecular concentration. The values obtained for σ_g at 532 nm were 6.51×10^{-16} cm^2 for the biprotonated TPP form and 7.137×10^{-16} cm^2 for the deprotonated one at a concentration of 35.1 μM. This is in conservative agreement with reported values of 0.8×10^{-17} cm^2 and 2.1×10^{-17} cm^2 for biprotonated and deprotonated *meso*-tetra(sulfonatophenyl) porphyrin solutions, respectively.[15] The addition of 10 μL of triethylamine again completely reversed the protonation process, restoring the deprotonated normal absorption spectrum for the TPP solutions. This confirms the equilibrium nature of the protonation mechanism.

Two characteristic emission peaks at 650 and 715 nm were observed for unsonicated (and therefore deprotonated) TPP samples in $CHCl_3$ with the luminescence maximum observed at 650 nm. This is typical porphyrin molecule emission. After sonication, the emission spectrum obtained from the same solution upon excitation at the same wavelength appeared very different. The fluorescence spectra for excitation at the Soret band of each solution, as depicted in Figure 4, presented a single maximum at 686 nm for the biprotonated TPP solutions after sonication. The two sharp emission bands of the TPP solution had been replaced by a single, broad emission band, centered at a wavelength of 685 nm. Upon the formation of a (1:1) composite with the SWNT, the emission was unchanged, and was typical of that observed from the protonated porphyrin. Negligible quenching was observed for composite solutions at concentrations below 6.5 μM. Emission spectra for solutions of ZnTPP with and without HiPCO SWNTs over the same concentration range displayed a similar red shift of 44.5 nm of the peak emission band from 603.5 to 648 nm upon sonication. Fluorescence was quenched in the Zn porphyrins relative to their free base counterparts. The low quantum yields for Zn-porphyrins reflect the high efficiency of nonradiative decay processes for metalloporphyrins, which is to be expected since this photochemistry arises only from high-lying excited states.

The UV−vis absorption spectrum for TPP/SWNT composite solutions in DMF is shown in Figure 2. It displays a normal absorption spectrum, with a Soret band observed at 416 nm. Neither the intensity nor the position of this band is altered upon solution irradiation or sonication, and the introduction of nanotubes into the system does not affect the absorption bands.

Two characteristic porphyrin PL bands were observed in the 600−750 nm region from the TPP and composite solutions in DMF (Figure 4A). Sonication and irradiation did not alter the emission spectrum of TPP in DMF, which displayed peaks at 650 and 717 nm. The emission spectrum is identical in the presence of nanotubes, with some quenching observed for the composite solutions. This quenching may be indicative of efficient energy transfer between the porphyrin molecules and the nanotube.[12] However, negligible quenching was observed for composite solutions below a concentration of approximately 2.5 μM for both TPP and ZnTPP, and as the quenching coincided with the onset of aggregation in the solutions, it could not conclusively be attributed to energy transfer to the nanotubes. An appreciable reduction in the porphyrin fluorescence for SWNT composites with both TPP and ZnTPP in DMF has been reported, with quenching factors of around 2.6 (SWNT/ZnTPP) and 5.9 (SWNT/TPP) observed.[16] In fact, we found the quenching factor to be concentration dependent, with values ranging from 1.27 to 12.6 being observed for TPP concentrations of 2.8 and 59 μM, respectively, and values of 1.26−5.6 being obtained for 2.5 and 53 μM ZnTPP solutions. The introduction of nanotubes into the system did not affect the onset of porphyrin aggregation for either molecule, which occurred for concentrations above 2.4 μM (Figure 4B).

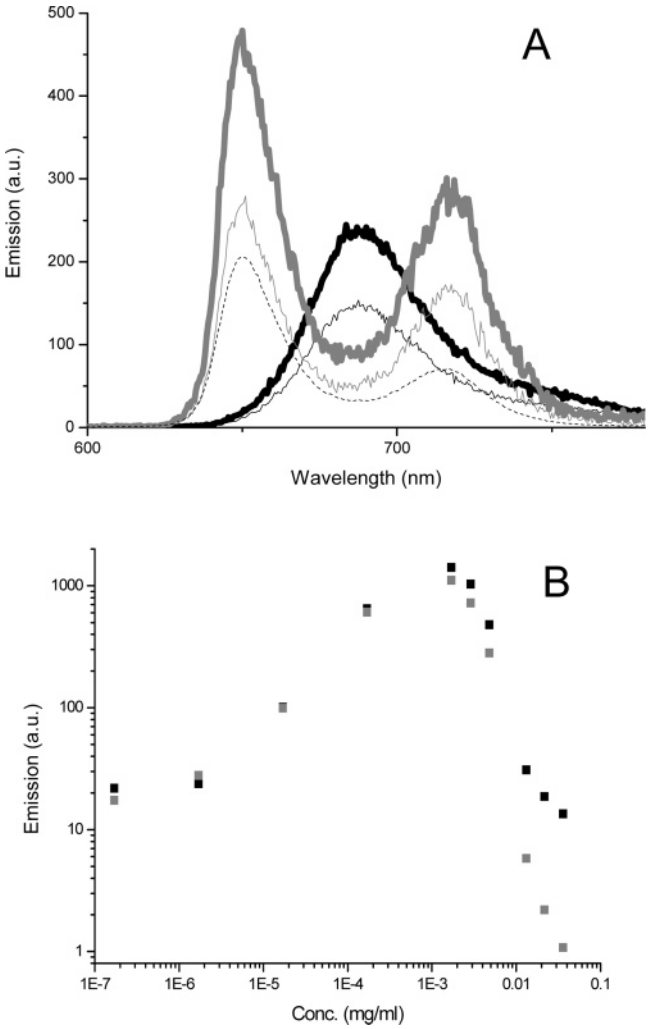

Figure 4. (A) PL spectrum of sonicated TPP (bold lines), unsonicated TPP (dashed line), and the corresponding sonicated TPP/SWNT (1:1) composite solutions (thin lines) in chloroform (black) [6.5 μM, $CHCl_3$, 25 °C] and DMF (gray) [7.6 μM, DMF, 25 °C] upon excitation at the absorption maxima. The PL spectra are unchanged upon the addition of nanotubes, with quenching being observed for composite solutions only at concentrations above 2.4 μM. (B) The plot of porphyrin (black) and composite (gray) emission intensities as a function of concentration showing that the presence of nanotubes does not delay the onset of aggregation-induced quenching at higher concentrations [DMF, 25 °C].

The open aperture of a *z*-scan experiment was used to measure the total transmittance through the samples.[17] Effective absorption coefficients were calculated as previously reported.[18,19] Normalized transmittance as a function of position z, $T_{Norm}(z)$, was given by

$$T_{\text{Norm}}(z) = \frac{\ln[1 + q_0(z)]}{q_0(z)} \text{ where } q_0(z) = \frac{q_{00}}{1 + (z + z_0)_2}$$

z_0 is the diffraction length of the beam, and $q_{00} = \beta_{\text{eff}} I_0 L_{\text{eff}}$, where $L_{\text{eff}} = [1 - \exp(-\alpha_0 L)]/\alpha_0$. β_{eff} is the effective intensity-dependent nonlinear absorption coefficient, and I_0 is the intensity of the light at focus. L_{eff} is known as the effective length of the sample defined in terms of the linear absorption coefficient, α_0, and the true optical path length through the sample, L. The imaginary third-order optical susceptibility $\text{Im}\{\chi^{(3)}\}$, is directly related to the intensity-dependent absorption coefficient β_I and is expressed as $\text{Im}\{\chi^{(3)}\} = n_0^2 \epsilon_0 c^2 \beta/\omega$, where n_0 is the linear refractive index, ϵ_0 is the permittivity of free space, c is the speed of light, and ω is the angular velocity of the incident light. All experiments described in this study were performed using 6 ns Gaussian pulses from a Q-switched Nd:YAG laser with energies of approximately 0.2−0.3 mJ per pulse.

The nonlinear values reported below were obtained by using this thin sample approximation and therefore constitute a lower limit of nonlinearity. The real sample length L (= 1 cm) is substantially larger than the depth of focus of the lens, and therefore the thick sample condition applies as described in ref 23. Since the derivations presented therein only refer to a Kerr-type nonlinearity and do not include nonlinear absorption effects, the equations presented above still represent a good approximation. The beam waist was found to range from 22 to 37 μm for all solutions studied.

Typical normalized energy transmission without an aperture (i.e., an open aperture) is shown in Figure 5 for a range of input energies. Both TPP and the metalloporphyrin ZnTPP were studied over the concentration range of 2.8−162.7 μM along with their SWNT composite solutions, with linear transmissions in the region of 50−80%. These solutions were prepared and studied in both chloroform and DMF.

All z-scans performed in this study exhibited a reduction in transmittance about the focus (Figure 5). This is typical of nonlinear absorption of incident light being induced in the sample. Figure 5 summarizes the nonlinear behavior observed with plots of normalized transmission as a function of distance from the focus shown for TPP solutions at low and high concentrations, with and without nanotubes present, at low and high irradiation energies. At higher incident intensities (> approximately 0.3 GW/cm^2), the transmission of the porphyrin solutions about the focus deviated from ideal RSA behavior. This was probably caused by porphyrin degradation due to local heating effects in the solution. Alternatively, since RSA is the principle nonlinear absorption mechanism for porphyrins, a similar deviation from ideal RSA behavior would be observed upon RSA saturation at high incident energies. However, because this effect was minimized during experiments by shaking the sample between scans, we feel that thermal degradation of the sample is the principle cause. The introduction of carbon nanotubes into the system completely prevented this degradation at all irradiances. Carbon nanotubes are known to be excellent thermal conductors and prevent local heating in these solutions by conducting heat away from areas of higher temperature. Nonlinear scattering is also likely to have contributed significantly to the optical limiting of the composite. It is well-known that carbon nanotubes exhibit excellent optical limiting properties, and the dominant mechanism for this behavior has been found to be absorption-induced nonlinear scattering.[10,21]

The nonlinear absorption coefficient, β_I, experienced by the incident pulses was determined from these spectra as a function of the on-focus intensity for all solutions in chloroform and in DMF. It was found that the introduction of the carbon nanotubes into the porphyrin solutions consistently led to a significant increase in the effective nonlinear absorption coefficient β_I, almost an order of magnitude in some cases. β_I was found to be nonstationary with respect to the on-focus intensity in all cases, both with and without nanotubes present. It was found that β_I decreases in magnitude with increasing focal intensity I_0 for all systems studied. Assuming very low irradiation intensities, where $I \ll I_{\text{sat}}$, then the intensity-dependent absorption coefficient may be written as $\alpha(I, I_{\text{sat}}, \kappa,) \approx \alpha_0(1 + (\kappa - 1) \approx I/I_{\text{sat}})$, which is the equation for a straight line of slope $(\kappa - 1)$. However, for a reverse saturable absorber, $\kappa > 1$ by definition, and so, where $I \ll I_{\text{sat}}$, one would expect the nonlinear absorption coefficient to increase as a function of I_0. This is not in agreement with the behavior of β_I as a function of I_0, which was measured here, and so these materials are not behaving as effective third-order nonlinear absorbers. The reduction in the nonlinear absorption coefficient could be due to some sort of saturation of the accessible energy levels under high-intensity pumping. Despite this, effective third-order nonlinear absorption coefficients, β_I, were estimated by suitably interpolating data such as that above for all compounds at (arbitrarily chosen) on-focus intensities of 0.4 GW cm^{-2} where possible.

The optical limiting curves are shown in Figure 6. Normalized transmission (T_{Norm}) was plotted as a function of the incident pulse energy density (J cm^{-2}). The nonlinear absorption coefficient $\alpha(F, F_{\text{sat}}, \kappa)$ was used to fit the normalized transmission as a function of this energy density to the data sets of all open aperture z-scans performed for each compound over a concentration range. Here, $\alpha(F, F_{\text{sat}}, \kappa)$ is derived from laser rate equations for the steady state and is defined as $\alpha(F, F_{\text{sat}}, \kappa) \approx \alpha_0(1 + F/F_{\text{sat}})^{-1}(1 + \kappa F/F_{\text{sat}})$. In this expression, F represents the energy density, F_{sat} is the saturation energy density, and κ is the ratio of the excited to ground-state absorption cross-sections $\sigma_{\text{ex}}/\sigma_0$. The parameters κ and F_{sat} were treated as free constants in the fitting algorithm. The plots of normalized transmission against pulse energy density for all solutions where the solid lines are theoretical fits to the experimental data are shown in Figures 6 and 7. The α_0, κ, and F_{sat} values for each compound are presented in Table 1.

Our results for TPP compare favorably with reported values for the benchmark molecule chloroindium phthalocyanine with the absorption cross-section κ calculated as being (30 ± 6) and β_I being approximately equal to 4.5×10^{-8} cm/W at an irradiation of 0.4 GW/cm^2.[20]

For comparison purposes, a full optical study was conducted on PPIX solutions for a range of concentrations. The normalized transmission plotted against the incident pulse energy density is shown in Figure 7 for porphyrin molecules in DMF, both with and without nanotubes present. The composite solutions (open symbols) were found to be much better optical limiters than the porphyrin solutions alone (filled symbols) for all solutions examined. The interpolated values of β_I for PPIX and its composite under 0.4 GW cm^{-2} irradiation were found to be 3.1×10^{-10} and 6.6×10^{-9} cm GW^{-1}, respectively, at a concentration of 7.8 μM. The introduction of the carbon nanotubes into the porphyrin solutions again led to a significant increase in the effective nonlinear absorption coefficient at all concentrations. The β_I of the protoporphyrin solutions was found to remain fairly constant as a function of concentration over the range studied, whereas it increased linearly with concentra-

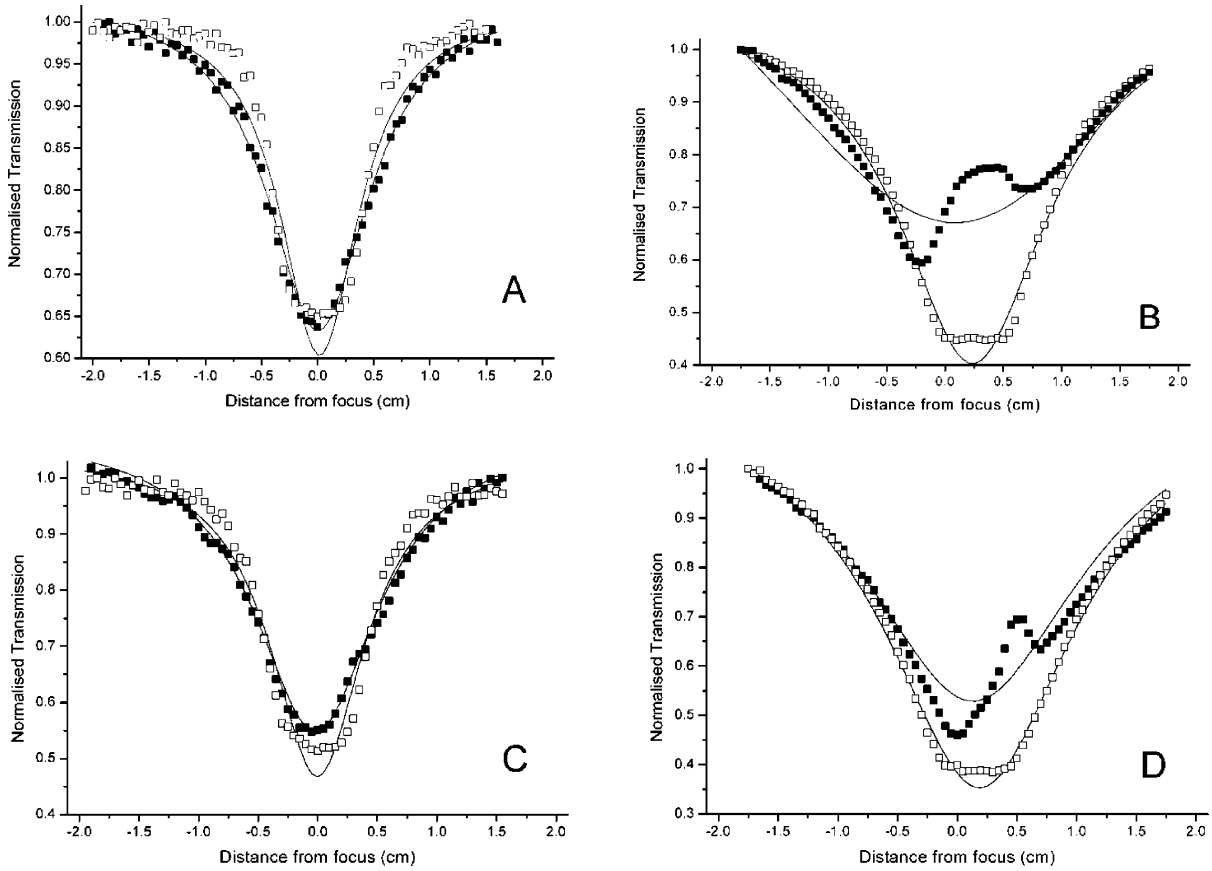

Figure 5. Plots of normalized transmission vs distance from the focus for TPP and composite solutions in DMF at (A) low concentration and low energy, (B) low concentration and high energy, (C) high concentration and low energy, and (D) high concentration and high energy. TPP solutions were at concentrations of 21 and 98 μM, and the composite concentrations were 7.6 and 2.7 μM, with on-focus intensities of (A) 0.138, (B) 1.23, (C) 0.136, and (D) 1.16 GW cm^{-2} for TPP solutions, and (A) 0.194, (B) 1.80, (C) 0.188, and (D) 1.58 GW cm^{-2} for composite solutions.

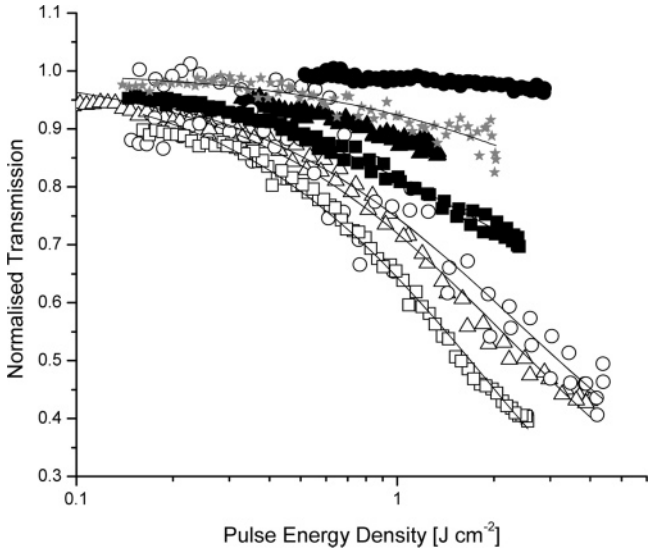

Figure 6. Plots of normalized transmission against pulse energy density for TPP (filled squares), TPP/SWNT (open squares), ZnTPP (filled circles), and ZnTPP/SWNT (open circles) solutions (12.7 μM); TPP (filled triangles), TPP/SWNT (open triangles) solutions (21.5 μM); and a 0.01 mg/mL SWNT suspension (gray stars). The composite solutions were found to be much better optical limiters than both the porphyrin solutions and SWNT alone.

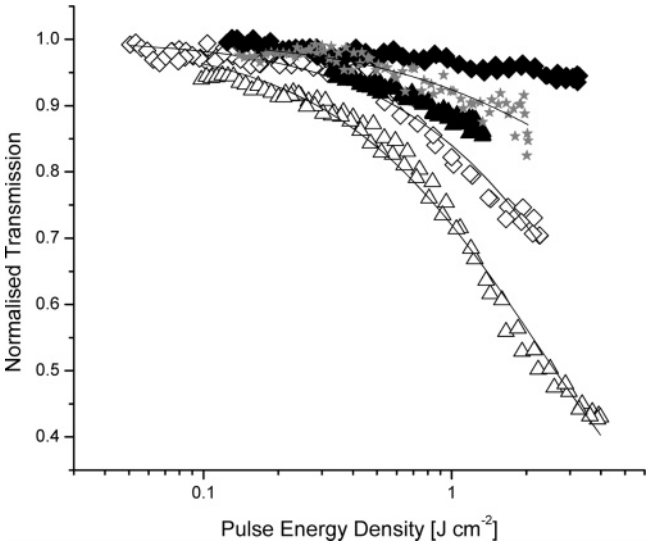

Figure 7. Plots of normalized transmission against pulse energy density for TPP (filled triangles), TPP/SWNT (open triangles), PPIX (filled diamonds), and PPIX/SWNT (open diamonds) solutions (21.5 μM, DMF, 25 °C) and a 0.01 mg/mL SWNT suspension (gray star). All plots shown were observed at an on-focus beam intensity, I_0, of approximately 0.2 GW cm^{-2}.

tion for the composite solutions. The nonlinear absorption coefficient, β_I, again decreased in magnitude as I_0 increased.

A dispersion of SWNTs in DMF (0.01 mg/mL) is also included in both Figures 6 and 7 for comparison purposes. It can clearly be seen that porphyrin composite solutions are far superior optical limiters to both porphyrins and SWNT alone for all porphyrins studied. If the optical limiting behavior of a composite solution was simply due to the combined optical dissipation of its nanotube and porphyrin components, the normalized transmission of that solution over a range of incident pulse energies would be equal to the product of the normalized

TABLE 1: Optical Coefficients for the Materials Measured

sample	c (μM)	solvent	α_0 (cm^{-1})	β_I (cm W^{-1})	Im{$X^{(3)}_{eff}$} (Esu)	I_0 (GW cm^{-2})	F_{sat} (J cm^{-2})	κ (σ_{ex}/σ_0)
TPP	12.7	$CHCl_3$	0.07	4.4×10^{-9}	1.5×10^{-12}	0.20	2.6 ± 0.1	11.2 ± 0.4
TPP+SWNT	12.7	$CHCl_3$	0.29	2.2×10^{-8}	7.7×10^{-12}	0.24	8.1 ± 0.9	15.0 ± 1.2
ZnTPP	11.5	$CHCl_3$	0.82	2.8×10^{-10}	9.8×10^{-14}	0.27	15.3 ± 11.0	1.3 ± 0.2
ZnTPP+SWNT	11.5	$CHCl_3$	0.29	9.8×10^{-9}	3.4×10^{-12}	0.41	5.4 ± 2.1	7.5 ± 1.8
TPP	21.5	DMF	0.11	2.8×10^{-9}	9.7×10^{-13}	0.13	2.1 ± 0.2	4.4 ± 0.2
TPP+SWNT	21.5	DMF	0.42	6.2×10^{-9}	2.1×10^{-12}	0.19	4.1 ± 0.3	3.6 ± 0.2
PPIX	21.5	DMF	0.22	4.5×10^{-10}	1.5×10^{-13}	0.31	1.2 ± 0.2	1.4 ± 0.0
PPIX+SWNT	21.5	DMF	0.72	6.7×10^{-9}	2.3×10^{-12}	0.21	16.3 ± 8.7	5.2 ± 2.0
SWNT	0.01 g/L	DMF	0.29	1.9×10^{-9}	6.4×10^{-13}	0.19	5.3 ± 2.2	2.7 ± 0.6

transmission spectra for each of the individual components over the same range of energies. However, this was not found to be the case, with the nanotube composites found to display superior optical limiting for all systems studied. This behavior is fully consistent with a recent study by Carroll et al.,[22] which reports on the enhanced nonlinear transmittance by an RSA dye blended with carbon nanotubes due to complementary nonlinear mechanisms. It was found that the blended suspensions offered superior performance to the individual constituent materials by compensating for their individual shortcomings with the others strengths. The addition of carbon nanotubes was found to greatly influence the nonlinear transmittance through the addition of a nonlinear scattering component to the RSA dye blends. It is evident that a similar mechanism is applicable for our porphyrin composite systems, with the nonlinear scattering behavior of the nanotubes extending functionality to high fluence protection. Particularly enhanced nonlinear dissipation was observed for the metalloporphyrin (ZnTPP) composite. This provides further evidence of interaction between carbon nanotubes and the porphyrin molecules. Thus, these noncovalently porphyrin-functionalized carbon nanotube solutions have enormous industrial potential for optical limiting applications.

Conclusions

Porphyrin molecules and their SWNT composites have been prepared such that the porphyrin−SWNT mass ratio was 1:1, and their linear and nonlinear optical properties have been investigated in DMF and chloroform. These noncovalently functionalized porphyrin−carbon nanotube composites were observed with TEM, where the amorphous porphyrin molecules were found to adhere to the nanotube surface. UV−vis absorption spectra were taken for TPP solutions in chloroform and DMF, with and without nanotubes present. Sonodegradation of composite solutions in chloroform during sample preparation resulted in the protonation of the porphyrin core nitrogen atoms, completely altering the porphyrin optical properties. Typical PL spectra were obtained from all systems, with negligible quenching observed for composite solutions in the absence of aggregation. We found the quenching factor to be concentration dependent, with values ranging from 1.27 to 12.6 being observed for TPP concentrations of 2.8 and 59 μM, respectively, and values of 1.26 to 5.6 being obtained for 2.5 and 53 μM ZnTPP solutions. This is in contrast to reported values of quenching factors of around 2.6 (SWNT/ZnTPP) and 5.9 (SWNT/TPP) observed in the porphyrin fluorescence for SWNT composites with both TPP and ZnTPP in DMF. The nonlinear behavior of porphyrin solutions was also measured using the z-scan technique in $CHCl_3$ and DMF, in the presence and absence of nanotubes. The nonlinear absorption coefficient, β_I, was found to decrease in magnitude as I_0 increased for all solutions. This is inconsistent with effective third-order nonlinear absorption behavior, and may be due to the saturation of the accessible energy levels under high-intensity pumping. The composite solutions were found to be superior optical limiters for all porphyrin systems studied, including metalloporphyrins, which do not themselves exhibit strong optical limiting behavior. This lends itself to interesting potential applications for these composite solutions.

Acknowledgment. The authors wish to acknowledge the support of the European Union in the form of the European Community's Human Potential Program under contract HPRNCT-2002-00192 [NANOTEMP]. Financial support from the Science Foundation Ireland (SFI) is also gratefully acknowledged.

References and Notes

(1) Murakami, H.; Nomura, T.; Nakashima, N. *Chem. Phys. Lett.* **2003**, *378*, 481−485.
(2) Li, H.; Zhou, B.; Lin, Y.; Gu, L.; Wang, W.; Fernando, K. A. S.; Kumar, S.; Allard, L. F.; Sun, Y. P. *J. Am. Chem. Soc.* **2004**, *126*, 1014−1015.
(3) Guldi, D. M.; Taieb, H.; Rahman, G. M. A.; Tagmatarchis, N.; Prato, M. *Adv. Mater.* **2005**, *17* (7), 871−875.
(4) Chen, J.; Collier, C. P. *J. Phys. Chem. B* **2005**, *109*, 7605−7609.
(5) Li, H.; Martin, R. B.; Harruff, B. A.; Carino, R. A.; Allard, L. F.; Sun, Y. P. *Adv. Mater.* **2004**, *16* (11), 896−900.
(6) Calvete, M.; Yang, G. Y.; Hanacket, M. *Synth. Met.* **2004**, *141*, 231−243.
(7) Henari, F. Z.; Blau, W. J.; Milgrom, L. R.; Yahioglu, G.; Phillips, D.; Lacey, J. A. *Chem. Phys. Lett.* **1997**, *267*, 229−233.
(8) Blau, W.; Byrne, H.; Dennis, W. M.; Kelly, J. M. *Opt. Commun.* **1985**, *56*, 25−29.
(9) Vivien, L.; Anglaret, E.; Riehl, D.; Hache, F.; Bacou, F.; Andrieux, M.; Lafonta, F.; Journet, C.; Goze, C.; Brunet, M.; Bernier, P. *Opt. Commun.* **2000**, *174*, 271−275.
(10) Mishra, S. R.; Rawat, H. S.; Mehendale, S. C.; Rustagi, K. C.; Sood, A. K.; Bandyopadhyay, R.; Govindaraj, A.; Rao, C. N. R. *Chem. Phys. Lett.* **2000**, *317*, 510−514.
(11) Riggs, J. E.; Walker, D. B.; Carroll, D. L.; Sun, Y. P. *J. Phys. Chem. B* **2000**, *104* (30), 7071−7076.
(12) Ní Mhuircheartaigh, É. M.; Giordani, S.; Blau, W. J. *J. Am. Chem. Soc.*, in press.
(13) Nikolaev, P.; Bronikowski, M. J.; Bradley, R. K.; Rohmund, F.; Colbert, D. T.; Smith, K. A.; Smalley, R. E. *Chem. Phys. Lett.* **1999**, *313*, 91−97.
(14) Baskaran, D.; Mays, J. W.; Zhang, X. P.; Bratcher, M. S. *J. Am. Chem. Soc.* **2005**, *127*, 6916−6917.
(15) Goncalves, P. J.; De Boni, L.; Barbosa Neto, N. M.; Rodrigues, J. J., Jr.; Zilio, S. C.; Borissevitch, I. E. *Chem. Phys. Lett.* **2005**, *407*, 236−241.
(16) Rahman, G. M. A.; Guldi, D. M.; Campidelli, S.; Prato, M. *J. Mater. Chem.* **2006**, *16*, 62−65.
(17) Sheik-Bahae, M.; Said, A. A.; Wei, T. H.; Hagan, D. J.; Van Stryland, E. W. *J. Quant. Electron.* **1990**, *26*, 760.
(18) O'Flaherty, S. M.; Hold, S. V.; Cook, M. J.; Torres, T.; Chen, Y.; Hanack, M.; Blau, W. J. *Adv. Mater.* **2003**, *15* (1), 19−32.
(19) O'Flaherty, S. M.; Hold, S. V.; Brennan, M. E.; Cadek, M.; Drury, A.; Coleman, J. N.; Blau, W. J. *J. Opt. Soc. Am. B* **2003**, *20* (1), 49−58.
(20) Perry, J. W.; Mansour, K.; Lee, I. Y. S.; Wu, X. L.; Bedworth, P. V.; Chen, C. T.; Ng, D.; Marder, S. R.; Miles, P.; Wada, T.; Tian, M.; Sasabe, H. *Science* **1996**, *273*, 1533−1536.
(21) Chen, P.; Wu, X.; Sun, X.; Lin, J.; Ji, W.; Tan, K. L. *Phys. Rev. Lett.* **1999**, *82*, 2548−2551.
(22) Webster, S.; Reyes-Reyes, M.; Pedron, X.; Lopez-Sandoval, R.; Terrones, M.; Carroll, D. L. *Adv. Mater.* **2005**, *17*, 1239−1243.
(23) Sheik-Bahae, M.; Said, A. A.; Hagan, D. J.; Soileau, M. J.; Van Stryland, E. W. *Opt. Eng.* **1991**, *30*, 1228−1235.